ELSEVIER

Biophysical Chemistry 72 (1998) 247–264

Biophysical Chemistry

Electrooptic analysis of macromolecule dipole moments using asymmetric reversing electric pulses

Astrid Bjørkøy, Arnljot Elgsaeter, Arne Mikkelsen *

Norwegian University of Science and Technology (NTNU), Norwegian Biopolymer Laboratory (NOBIPOL), Department of Physics, Sem Saelandsvei 9, N-7034 Trondheim, Norway

Received 25 November 1997; revised 15 January 1998; accepted 15 January 1998

Abstract

The use of symmetric reversing electric field pulses in electrooptic studies of rigid macromolecules in order to determine the ratio between the permanent and the induced dipole moments is well established. Application of this method to studies of small macromolecules requires a field reversal time of only a few nanoseconds. No high current pulse generator capable of producing symmetric kV pulses with such a short reversal time is available for studies of small macromolecules in physiological salt solutions, but it has long been known how to make such reversing pulses that are asymmetric. In order to take advantage of the opportunity offered by the latter fact, we here present a theoretical analysis in the thermal domain of the electrooptic properties of solutions containing rigid macromolecules with axial symmetry when exposed to asymmetric reversing electric field pulses. The analytical expressions needed for quantitative determination of the ratio between the permanent and the induced electric dipole moments of rigid macromolecules using electrooptic data obtained employing reversing electric pulses with given asymmetry are presented. The feasibility of this new approach is demonstrated by including experimental electric birefringence data for a 12 kDa protein (segment 14 of α-spectrin from Drosophila brains) in near physiological salt solutions obtained using a coaxial cable pulser producing 2 μs long pulses with a reversal time of about 15 ns.

Keywords: Electrooptics; Dichroism; Birefringence; Electric dipole moments

1. Introduction

Electrostatics play an important role in determining the structure and function of macromolecules, such as proteins, glycoproteins and nucleic acids, because important aspects of the intra- and inter-molecular interactions often are dominated by the electrostatic forces. Because of the long range and the complex effects of these forces on the macromolecules themselves, a theoretical calculation of the electric charge distribution and thus the dipole moments of a protein is rather complicated [1]. Significant progress has been made in this field during

* Corresponding author. Tel.: +47-73593433; fax: +47-73597710; e-mail: arne.mikkelsen@phys.ntnu.no

0301-4622/98/$19.00
PII S0301-4622(98)00110-0

the last few years [2], but it is still important to be able to verify experimentally that the results predicted by such theoretical analyses are indeed quantitatively valid.

Studies of electrically-induced birefringence and dichroism provide detailed information about the electric and optic properties of macromolecules, as well as about their size and flexibility. When an external electric field is applied to a macromolecule solution, the favoured alignment of the molecules parallel to the field is caused by the interaction between the external electric field and the permanent and/or induced electric dipole moments. The rise and decay times of this alignment contain information about the molecular dimensions. The dipole moments of macromolecules are routinely determined by measuring the transient and stationary dichroism or birefringence when the external electric field is changed instantaneously I) from zero to a constant non-zero value or II) from a constant non-zero value to the same non-zero negative value. These two methods can, in principle, yield the same information about the dipole moments and can therefore be used to obtain independent estimates of the same molecular parameters. The latter method is referred to as the symmetric reversing pulse technique and is the most widely used of these two techniques for obtaining the ratio between the permanent and the induced dipole moments [3–5].

Commercial pulse generators providing symmetric reversing kV electric pulses, where the field reversal takes place within a fraction of 1 μs and the electric current is less that a few amperes, are readily available. But no high voltage pulse generator that provides 100 A or higher current pulses with symmetric field reversal within a few nanoconds has yet been reported [6]. Asymmetric reversing 10 kV or higher electric pulses providing a current of 100 A or higher, and having reversal time down to a few ns can readily be generated using the coaxial cable discharge technique [7,8]. Reversing pulses are obtained when the terminating electric impedance is smaller than the characteristic impedance of the coaxial cable.

In order to take advantage of the opportunity offered by the latter fact, we hereby report on a quantitative theoretical analysis of the birefringence/dichroism of macromolecule solutions exposed to asymmetric reversing electric field pulses. Our theoretical analysis shows that asymmetric reversing pulses can be used successfully to obtain estimates of the ratio between the permanent and the induced dipole moments provided that the signal-to-noise ratio of the electrooptic data is adequate. The theoretical analysis predicts that the signal-to-noise ratio decreases when the asymmetry of the reversing pulse is increased. To demonstrate the feasibility of using asymmetric reversing electric pulses to study the electrooptic properties of small macromolecules, we have included experimental birefringence data for a 12 kDa protein (segment 14 of α spectrin from Drosophila brains) in near physiological salt solutions.

2. Theory

2.1. Electric birefringence and dichroism

Here, we will limit the analysis to rigid macromolecules with fore–aft and axial symmetry (e.g., ellipsoids) and electric potential energy U that is small compared to the thermal energy $k_B T$, where k_B is the Boltzmann constant and T is the absolute temperature. For given macromolecule electric dipole moments, this determines the upper limit of the electric field for which our final results are valid.

In our analysis, we use a particle-fixed local coordinate system that may translate, but not rotate, relative to the fixed laboratory coordinate system (Fig. 1).

The origin of the particle-fixed coordinate system is located at the center of diffusion of the particle, and the orientation of the macromolecule axis of rotational symmetry is specified by the spherical coordinates θ and ϕ. The homogeneous external electric field $\vec{E}$ is parallel to the z-axis. This means that the angular distribution function $f(\theta,\phi,t)$ describing the probability of finding the molecular axis in a space element $\mathrm{d}\Omega = \sin\theta \mathrm{d}\theta \mathrm{d}\phi$ at time t is independent of ϕ.

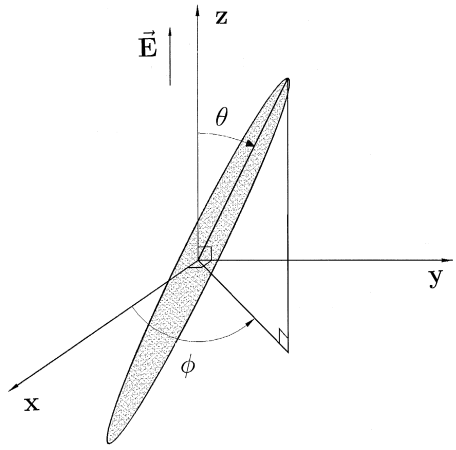

Fig. 1. Schematic illustration of the spherical coordinates associated with each molecule. The homogeneous external electric field $\vec{E}$ is parallel to the z-axis of the local Cartesian coordinate system with origin at the diffusion center of each molecule. This local coordinate system may translate relative to the space-fixed laboratory coordinate system. The molecule is oriented with its long axis at an angle θ with respect to the external electric field. The azimuth angle is denoted by ϕ.

The equilibrium value of the probability density function $f(\theta)$ can be calculated according to the Boltzmann formula:

$$f(\theta) = \frac{\exp\{-U(\theta)/(k_B T)\}}{\int_0^{\pi} \exp\{-U(\theta)/(k_B T)\} 2\pi \sin\theta \mathrm{d}\theta} \tag{1}$$

The potential energy of the macromolecule in the electric field arises from the two terms, $U_1(\theta)$ and $U_2(\theta)$. The first term is the electric potential associated with the permanent dipole moment and the second term is due to the induced dipole moment:

$$U(\theta) := U_1(\theta) + U_2(\theta) = -\mu \boldsymbol{E} \cos\theta - \frac{v}{2}\left(\hat{\alpha}_1 \cos^2\theta + \hat{\alpha}_2 \sin^2\theta\right)\boldsymbol{E}^2 \tag{2}$$

where μ is the permanent dipole moment and v is the macromolecule volume [4]. The internal electric field of the molecule is here for simplicity assumed to equal the electric field E in the surrounding medium. Parameters $\hat{\alpha}_1$ and $\hat{\alpha}_2$ are the electrical polarizabilities per unit volume of the macromolecule at frequencies below approximately 1 GHz when the field is parallel and perpendicular to the axis of rotational symmetry, respectively. The expression for the potential $U(\theta)$ must be modified if induced dipole effects with long characteristic decay times giving rise to properties qualitatively similar to those of a permanent dipole, are taken into account [3]. If the macromolecule is a rodlike macroion, an additional energy term must be considered in Eq. (2) because of the distortion of the ion-atmosphere near the macromolecule and the resulting coupled rotational and ion-atmosphere dynamics [9,10]. For simplicity, the ion-atmosphere distortion and other slow induced dipole effects have been neglected in our calculations.

The applied electric field produces optical anisotropy. When the particles/molecules become aligned in the medium, incident light with electric field vectors parallel and perpendicular to the external electric field vector will propagate at different velocities. The birefringence of the medium is defined as

$$\Delta n := n_{\parallel} - n_{\perp} \tag{3}$$

where $n_{\parallel}$ and $n_{\perp}$ are the refractive indices for light polarized parallel and perpendicular relative to the external field, respectively. The refractive indices depend on the electrical polarizability of the macromolecules at optical frequencies (10^6 GHz).

A solution containing aligned macromolecules may also exhibit birefringence when each individual molecule does not possess intrinsic birefringence. This is called form birefringence, but for most dilute macromolecule solutions, the form birefringence is much smaller than the intrinsic birefringence. The form birefringence is therefore ignored in the following.

It can be shown [4] that the contribution to the total birefringence of a medium containing N macromolecules/particles per unit volume, all with polar angle θ, equals:

$$\Delta n(\theta) = \Delta n_s \left(\frac{3\cos^2\theta - 1}{2} \right) = \frac{N_V (\hat{\alpha}_1 - \hat{\alpha}_2)}{2 n_0 \varepsilon_0} \left(\frac{3\cos^2\theta - 1}{2} \right) \tag{4}$$

where Δn_s is called the saturation birefringence. Parameter n_0 equals the refractive index of the solution, and ε_0 is the permittivity of vacuum.

In order to obtain the total birefringence Δn, the birefringence probability density function $\Delta n(\theta)$ is integrated over the whole angular space. This yields:

$$\Delta n = \frac{N_V (\hat{\alpha}_1 - \hat{\alpha}_2)}{2 n_0 \varepsilon_0} \int_0^{\pi} f(\theta) \left(\frac{3\cos^2\theta - 1}{2} \right) 2\pi \sin\theta \, d\theta \tag{5}$$

In the following, our attention will be focused on the angular probability density function $f(\theta)$. It can be shown [4] that the expression for the electric dichroism of a solution containing rigid macromolecules is analogous to Eq. (5) and that for each theoretical expressions derived in the following for electric birefringence there exists a corresponding expression that is valid for electric dichroism.

2.2. Angular space diffusion equation

The angular space equation of change describing the Brownian diffusion process biased by the applied electric field may be written as [11,12]:

$$\frac{\partial f(\theta,t)}{\partial t} = D_R \nabla_\theta^2 f(\theta,t) - \nabla_\theta \cdot \left[\dot{\theta} f(\theta,t) \vec{\delta}_\theta \right] \tag{6}$$

where D_R is the rotational diffusion coefficient of the molecules around their transverse axes, $\dot{\theta}$ is the angular drift velocity due to the torque T_θ generated by the external electric field and $\vec{\delta}_\theta$ is the unit vector in θ direction. Using the definition of the rotational friction coefficient f_R and the Nernst–Einstein relation, $\dot{\theta}$ may be expressed as:

$$\dot{\theta} = \frac{1}{f_R} T_\theta = \frac{D_R}{k_B T} T_\theta = -\frac{D_R}{k_B T} \frac{\partial U}{\partial \theta} \tag{7}$$

Employing spherical coordinates and the result in Eq. (7), the θ-space equation of change reads:

$$\frac{1}{D_R} \frac{\partial f(\theta,t)}{\partial t} = \frac{1}{\sin\theta} \frac{\partial}{\partial \theta} \left(\sin\theta \frac{\partial f(\theta,t)}{\partial \theta} \right) + \frac{1}{k_B T} \left[\frac{\partial U}{\partial \theta} \frac{\partial f(\theta,t)}{\partial \theta} + \frac{f(\theta,t)}{\sin\theta} \frac{\partial}{\partial \theta} \left(\sin\theta \frac{\partial U}{\partial \theta} \right) \right] \tag{8}$$

Use of Eq. (2) for potential $U(\theta)$ and introducing a new variable $u = \cos\theta$ in Eq. (8) yield

$$\frac{1}{D_R} \frac{\partial f}{\partial t} = (1-u^2) \frac{\partial^2 f}{\partial u^2} - 2u \frac{\partial f}{\partial u} - (1-u^2)[p + qu] \frac{\partial f}{\partial u} + [2pu + q(3u^2 - 1)] f \tag{9}$$

where

$$p := \frac{\mu E}{k_B T} \tag{10}$$

is the dimensionless permanent dipole moment per macromolecule and

$$q := \frac{v(\hat{\alpha}_1 - \hat{\alpha}_2)E^2}{k_B T} \tag{11}$$

is the dimensionless induced dipole moment per macromolecule. The following trial solution for $f(u,t)$ proves to be useful

$$f(u,t) = \sum_{n=0}^{\infty} a_n(t) P_n(u) = a_0(t) + a_1(t)u + a_2(t)\left(\frac{3u^2 - 1}{2}\right) + \cdots, \tag{12}$$

where $P_n(u)$ is the Legendre polynomial of order n.

Substituting the trial solution for $f(\theta)$ into Eq. (5), it can be seen that the only term that contributes to the total birefringence/dichroism is the one involving $P_2(\cos\theta) = (3\cos^2\theta - 1)/2$. This is so because the Legendre polynomials are orthogonal functions, that is

$$\int_{-1}^{+1} P_n(u) P_m(u) \mathrm{d}u = \delta_{nm} \tag{13}$$

where δ_{nm} is the Kroenecker delta. The birefringence given by Eq. (5) therefore equals

$$\Delta n = \frac{Nv(\hat{\alpha}_1 - \hat{\alpha}_2)}{2 n_0 \varepsilon_0} a_2(t) \tag{14}$$

revealing that only $a_2(t)$ contributes to the birefringence. Also the dichroism of a solution can be shown to be proportional to $a_2(t)$.

When the trial solution given in Eq. (12) and the Legendre's differential equation

$$(1 - u^2)\frac{\mathrm{d}^2 P_n(u)}{\mathrm{d}u^2} - 2u\frac{\mathrm{d}P_n(u)}{\mathrm{d}u} + n(n+1)P_n(u) = 0 \tag{15}$$

are introduced into Eq. (9), it follows that

$$\frac{1}{D_R}\sum_{n=0}^{\infty}\frac{\mathrm{d}a_n(t)}{\mathrm{d}t}P_n(u) = -\sum_{n=0}^{\infty} n(n+1)a_n(t)P_n(u) - (1-u^2)[p + qu]\sum_{n=0}^{\infty} a_n(t)\frac{\mathrm{d}P_n(u)}{\mathrm{d}u} + \left[2pu + q(3u^2 - 1)\right]\sum_{n=0}^{\infty} a_n(t)P_n(u) \tag{16}$$

Both $\mathrm{d}P_n(u)/\mathrm{d}u$ and u can be eliminated from Eq. (16), using the recursion formulas

$$(1 - u^2)\frac{\mathrm{d}P_n(u)}{\mathrm{d}u} = nP_{n-1}(u) - nuP_n(u)$$

$$(2n+1)uP_n(u) = (n+1)P_{n+1}(u) + nP_{n-1}(u)$$

Subsequent multiplication of the resulting equation with $P_m(u)$ and integration over u from -1 to $+1$ yield the following set of coupled differential equations for determination of the coefficients $a_0(t)$, $a_1(t)$ and $a_2(t)$:

$$\begin{aligned}
\frac{\mathrm{d}}{\mathrm{d}t}a_0(t) &= 0 \\
\frac{1}{D_\mathrm{R}}\frac{\mathrm{d}}{\mathrm{d}t}a_1(t) &= 2pa_0 - 2(1-q/5)a_1(t) - (2p/5)a_2(t) \\
\frac{1}{D_\mathrm{R}}\frac{\mathrm{d}}{\mathrm{d}t}a_2(t) &= 2qa_0 + 2pa_1(t) - 2(3-q/7)a_2(t)
\end{aligned} \tag{17}$$

where the higher order terms a_3, $a_4, \ldots$ have been ignored. This corresponds to ignoring terms of higher order than two in p and one in q, or, equivalently, terms of higher order than two in E. These equations are therefore valid only for values of the external electric field smaller than a certain maximum. Using matrix notation, Eq. (17) can be rewritten as

$$\frac{1}{D_\mathrm{R}}\frac{\mathrm{d}}{\mathrm{d}t}\begin{pmatrix} a_1(t) \\ a_2(t) \end{pmatrix} = \begin{pmatrix} -2(1-q/5) & -2p/5 \\ 2p & -2(3-q/7) \end{pmatrix}\begin{pmatrix} a_1(t) \\ a_2(t) \end{pmatrix} + 2a_0\begin{pmatrix} p \\ q \end{pmatrix} \tag{18}$$

or, in a more compact notation, $(1/D_\mathrm{R})\dot{\vec{a}} = \vec{\vec{\mathbf{A}}}\cdot\vec{a} + \vec{a}_0$; where the terms can be identified by comparison with Eq. (18).

It is important to note here that this set of coupled first order differential equations is linear or non-linear depending on whether $p = p(U(t))$ and $q = q(U(t))$ are constants or not. When the only time dependence of $U(t)$ consists of instantaneous changes from one constant value to another, it is possible to select all time intervals in such a manner that for each time interval Eq. (18) will be linear (constants p and q). When the changes in $U(t)$ are not instantaneous there will at least be some time intervals where Eq. (18) is non-linear.

Solving the set of coupled first order differential equations given in Eq. (18) is equivalent to solving the linearized angular space diffusion equation in the thermal domain for electric birefringence and dichroism.

2.3. General solution when p and q are constants

The general solution of Eq. (18) for time interval where the electric field and thus p and q are constants equals

$$\begin{pmatrix} a_1(t) \\ a_2(t) \end{pmatrix} = \begin{pmatrix} b_1 & b_2 \\ 1 & 1 \end{pmatrix}\begin{pmatrix} c_1 & \exp\{D_\mathrm{R}\lambda_1 t\} \\ c_2 & \exp\{D_\mathrm{R}\lambda_2 t\} \end{pmatrix} + \begin{pmatrix} a_1(\infty) \\ a_2(\infty) \end{pmatrix} \tag{19}$$

which can be rewritten as $\vec{a} = \vec{\vec{\mathbf{B}}}\cdot\vec{c} + \vec{a}_\infty$. The parameters λ_1, λ_2, b_1 and b_2 can be determined by solving the homogeneous part of Eq. (18). The task is then reduced to solving a standard eigenvalue problem. The characteristic equation yields the following eigenvalues of matrix $\vec{\vec{\mathbf{A}}}$:

$$\lambda_1 = -2 + \frac{2}{5}q - \frac{1}{5}p^2 \tag{20}$$

$$\lambda_2 = -6 + \frac{2}{7}q + \frac{1}{5}p^2 \tag{21}$$

The corresponding eigenvectors equal

$$\vec{b}_1 = \begin{pmatrix} b_1 \\ 1 \end{pmatrix} = \begin{pmatrix} \frac{2}{p}\left(1 + \frac{q}{35}\right) \\ 1 \end{pmatrix} \tag{22}$$

$$\vec{b}_2 = \begin{pmatrix} b_2 \\ 1 \end{pmatrix} = \begin{pmatrix} \frac{p}{10}\left(1 - \frac{q}{35}\right) \\ 1 \end{pmatrix} \tag{23}$$

These eigenvectors are the column vectors of matrix $\vec{\vec{\mathbf{B}}}$. Terms of higher order than two in p and one in q are ignored.

As $t \to \infty$, $a_1(t) = a_1(\infty)$ and $a_2(\infty)$, the left hand side of Eq. (18) vanishes and the stationary values equal

$$a_1(\infty) = pa_0 \tag{24}$$

$$a_2(\infty) = \frac{1}{3}(p^2 + q)a_0 \tag{25}$$

where terms of higher order than two in p and one in q are neglected. The remaining parameters c_1 and c_2 are determined by the initial conditions

$$\begin{pmatrix} a_1(0) \\ a_2(0) \end{pmatrix} = \begin{pmatrix} b_1 & b_2 \\ 1 & 1 \end{pmatrix}\begin{pmatrix} c_1 \\ c_2 \end{pmatrix} + \begin{pmatrix} a_1(\infty) \\ a_2(\infty) \end{pmatrix} \tag{26}$$

which yields that

$$c_1 = -\frac{1}{b_2 - b_1}\{[a_1(0) - a_1(\infty)] - b_2[a_2(0) - a_2(\infty)]\} \tag{27}$$

$$c_2 = \frac{1}{b_2 - b_1}\{[a_1(0) - a_1(\infty)] - b_1[a_2(0) - a_2(\infty)]\} \tag{28}$$

Introducing the amplitudes and the decay constants given by Eqs. (20)–(23) in Eqs. (27) and (28), the general expression for $a_2(t)$ becomes

$$a_2(t) = a_2(\infty) + \frac{p}{2}[a_1(0) - a_1(\infty)]\exp\{-2D_R t\} + \left\{-\frac{p}{2}[a_1(0) - a_1(\infty)] + [a_2(0) - a_2(\infty)]\right\} \times \exp\{-6D_R t\}, \tag{29}$$

when parameters p and q are constants and it is assumed that $p^2 \ll 1$ and $q \ll 1$.

2.4. Special solutions when p and q are constants

For an instantaneous onset of the electric field at time $t = 0$ we have that

$$E(t) := \begin{cases} 0 & \text{if } t < 0 \\ E_0 & \text{if } t \geq 0 \end{cases} \tag{30}$$

yielding the following initial conditions:

$$a_0 = 1,\ a_1(0) = 0 \text{ and } a_2(0) = 0. \tag{31}$$

This, in turn, gives the stationary values

$$a_1(\infty) = p_0 \tag{32}$$

$$a_2(\infty) = \frac{1}{3}\left(p_0^2 + q_0\right) \tag{33}$$

where $p_0 \coloneqq \mu E_0/(k_B T)$ and $q_0 \coloneqq \upsilon(\hat{\alpha}_1 - \hat{\alpha}_2)E_0^2/(k_B T)$ are the equilibrium values of p and q for the given value E_0. Inserted in Eq. (29), this yields that the rise of the relative birefringence/dichroism following an instantaneous onset of the electric field equals

$$\frac{a_2(t)}{a_2(\infty)} = 1 - \frac{3p_0^2}{2\left(p_0^2 + q_0\right)}\exp\{-2D_R t\} + \frac{p_0^2 - 2q_0}{2\left(p_0^2 + q_0\right)}\exp\{-6D_R t\} \tag{34}$$

An asymmetric reversing electric pulse may be described as

$$E(t) \coloneqq \begin{cases} E_0 & \text{if } t < 0 \\ -\xi E_0 & \text{if } t \geq 0 \end{cases} \tag{35}$$

where $\xi \epsilon [0,1]$ is the symmetry parameter, sometimes also called the reflection parameter. Assuming that we have thermodynamic equilibrium before field reversal, this yields the initial conditions:

$$a_0 = 1,\ a_1(0) = p_0 \text{ and } a_2(0) = \frac{1}{3}\left(p_0^2 + q_0\right) \tag{36}$$

For the reversing field $p = -\xi p_0$ and $q = \xi^2 q_0$, we find that

$$a_1(\infty) = -\xi p_0 \tag{37}$$

$$a_2(\infty) = \frac{1}{3}\xi^2\left(p_0^2 + q_0\right) \tag{38}$$

When these results are inserted in Eq. (29), we get

$$\frac{a_2(t)}{a_2(0)} = \xi^2 + \frac{3}{2}(1+\xi)\xi\frac{p_0^2}{p_0^2 + q_0}\left[\exp\{-6D_R t\} - \exp\{-2D_R t\}\right] + \left(1 - \xi^2\right)\exp\{-6D_R t\} \tag{39}$$

A single rectangular electric pulse can be viewed as a special case of Eq. (35), where $\xi = 0$. The corresponding modification of Eq. (39) yields that the decay of the relative birefringence/dichroism, then equals

$$\frac{a_2(t)}{a_2(0)} = \exp\{-6D_R t\} \tag{40}$$

In the special case of a symmetric reversing electric pulse, $\xi = 1$, Eq. (39) takes the form

$$\frac{a_2(t)}{a_2(0)} = 1 + \frac{3p_0^2}{p_0^2 + q_0}\left[\exp\{-6D_R t\} - \exp\{-2D_R t\}\right] \tag{41}$$

Eqs. (34), (40) and (41) are in agreement with the well-known equations of Benoit [11], Tinoco [12], and Tinoco and Yamaoka [3]. Eq. (39) describing the time development of birefringence/dichroism for asymmetric reversing electric pulses has, to our knowledge, not been derived previously.

2.5. Time dependent p and q

If the reversing electric pulse is not ideal as in Eq. (35), but exhibits a non-zero reversal time, Eq. (35) must be replaced by

$$E(t) = \begin{cases} E_0 & \text{if } t < 0 \\ E_0\left[-\xi + \sum_{i=1}^{N} c_i \exp(-t/\tau_i)\right] & \text{if } t \geq 0 \end{cases} \tag{42}$$

where the field reversal is modelled as a sum of exponential decays with decay times τ_i and associated amplitudes c_i, where $\sum c_i = 1 + \xi$. The parameters p and q are then no longer constants and for a reversing electric field, we get

$$p(t) = p_0\left[-\xi + \sum_{i=1}^{N} c_i \exp(-t/\tau_i)\right] \tag{43}$$

$$q(t) = q_0\left[-\xi + \sum_{i=1}^{N} c_i \exp(-t/\tau_i)\right]^2 \tag{44}$$

It is important to note that for non-ideal reversing pulses Eq. (18) becomes non-linear and that Eq. (29) in general no longer is a solution of Eq. (18). In the general case, the non-linear version of the set of coupled differential equation, Eq. (18), has no analytic solution and $a_2(t)$ can only be obtained using numerical integration methods. The quantitative consequences of neglecting the non-linearity associated with non-ideal electric field pulses are presented elsewhere [13].

3. Materials and methods

3.1. Instrumentation

The electric birefringence instrument used in this study is shown schematically in Fig. 2. For further technical details see the work of Bjørkøy [14].

Electric pulses are generated across the Kerr cell using the coaxial cable discharge technique [7,8,15]. When the pneumatically-controlled spark gap fires, the cable negative high voltage is discharged through the electric load impedance to electric ground. A Suhner RG-218/U50 $\pm$ 2 Ω coaxial cable is used in the experiments described here. The cable length is 200 m, yielding a pulse duration of 2 μs. Because of the geometry of the spark gap, the coaxial cable can only be charged up to 18–20 kV despite that the coaxial cable itself can safely be charged to much higher voltages. The load impedance consists of the Kerr cell and a compensation cell coupled in parallel. The required Kerr cell sample volume is 600 μl. The volume of the compensation cell equals 4.2 ml. Both of these two cells have cylindrical geometry. The load impedance can be adjusted by

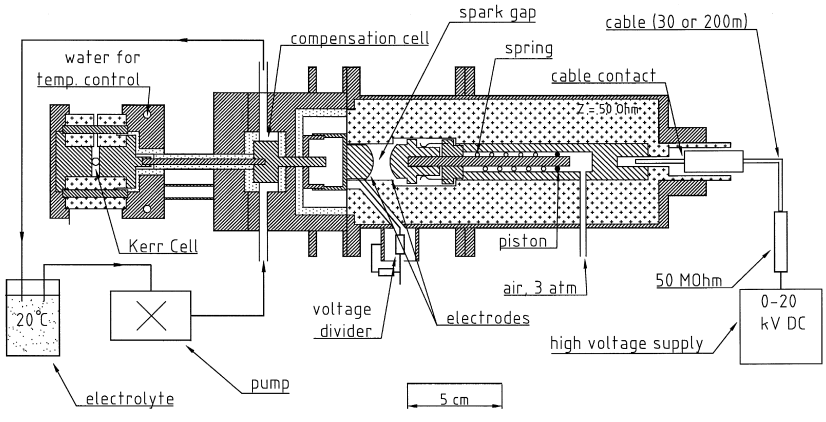

Fig. 2. A schematic illustration of the Kerr cell and the coaxial cable high voltage pulser used in the feasibility study reported here. The optical system and computerized data acquisition system are not shown. For more technical details, see the work of Bjørkøy [14].

changing the conductivity of the solutions in these cells. One single rectangular pulse is generated per coaxial cable discharge when the load impedance equals 50 Ω (impedance matching). When the load impedance is smaller than 50 Ω (impedance mismatching), multiple reversing pulses are obtained per coaxial cable discharge. The Kerr cell is under temperature control (2–40°C). The compensating electrolyte is kept at room temperature (20°C) and circulates to ensure removal of air bubbles in the compensation chamber.

The optical detection system is in principle identical to the systems described repeatedly in the literature [4,16,17]. The light source is an Omnichrome Argon laser, model 543-AP, operated at wavelength 488 nm. The polarizer, analyser, and the quarter-wave plate in front of the analyser are all obtained from B. Halle (Berlin, Germany). The electric field of the incident light is oriented 45° relative to the direction of the electric field across the Kerr cell. Light intensity variations caused by the birefringent protein sample are detected by a RCA 1P28 photomultiplier tube (PM-tube). In the quadratic detection mode, the polarizer and analyser are crossed. In the linear detection mode, the analyser is rotated a small angle away from the crossed orientation.

Both the electric excitation pulse and the signal from the PM-tube can be displayed on a Tektronix TDS 620 digital storage oscilloscope for which the minimum time between two subsequent data acquisitions equals 0.5 ns. Data stored in the oscilloscope can be transferred to a personal computer for further analysis using a HPIB-bus communication line.

3.2. Preparation of segment 14 of Drosophila α-spectrin

The recombinant fragment of a cDNA clone encoding segment 14 of *Drosophila* α-spectrin (Dα14) was expressed in *Escherichia coli* (strain 71-18) as a glutathione transferase-spectrin fusion protein [18]. The purification process included affinity purification on glutathione–agarose beads and cleavage of the fusion protein with thrombin. The purity of the protein solution was checked by SDS polyacrylamide gel electrophoresis. One litre of *E. coli* culture gave about 10 mg protein. Because of some tendency to self-associate, two single segments may form a dimer [19]. Gel filtration separation to remove dimers was performed at 4°C on Sephacryl S-100 HR using a XK 16/100 column from Pharmacia. The spectrin segment solution was applied to the column after concentration and dialysis against the eluent buffer containing 10 mM HEPES, pH 7.35/100 mM NaCl. The volume of the applied sample was 2.8 ml and the sample concentration was 2.5 mg/ml. The column was eluated at a flow rate of 15 ml/h. The dimer-containing peak eluated at 99 ml and the monomer-containing peak at 116 ml. A fraction of the latter peak was then dialyzed against 5 mM HEPES, pH 7.35/1 mM NaCl. Spectrin concentrations were determined by UV-light absorbance measurements using a specific absorbance of $A^{1\ \mathrm{cm}}_{1\%}(280\ \mathrm{nm}) = 10.1$, assuming that the specific absorbance of segment 14 is the same as for the native spectrin chains [20]. Electric birefringence was measured at 4 ± 1°C.

4. Results and discussion

4.1. Theoretical predictions of electrooptic properties

Plots of the relative birefringence/dichroism predicted by Eq. (39) for symmetry parameters $\xi = 1.0$, 0.7, 0.5 and 0.3 are shown in Fig. 3. For each value of ξ, the birefringence/dichroism is calculated for different values of p_0^2/q_0, ranging from 0 to 1000. The plots are given on dimensionless time scale, $t^* = D_R t$, and it can be seen from Eq. (39) that the t^*-dependence of the relative birefringence/dichroism, except for the scaling parameters, is the same for all values of the rotational diffusion coefficient D_R. On such a plot, the minimum value of $a_2(t^*)/a_2(0)$ is therefore independent of D_R and depends only on p_0^2/q_0. Hence, an estimate of p_0^2/q_0 for a given ξ can be obtained by simply determining experimentally the minimum value of $\Delta n_2(t^*)/\Delta n_2(0)$.

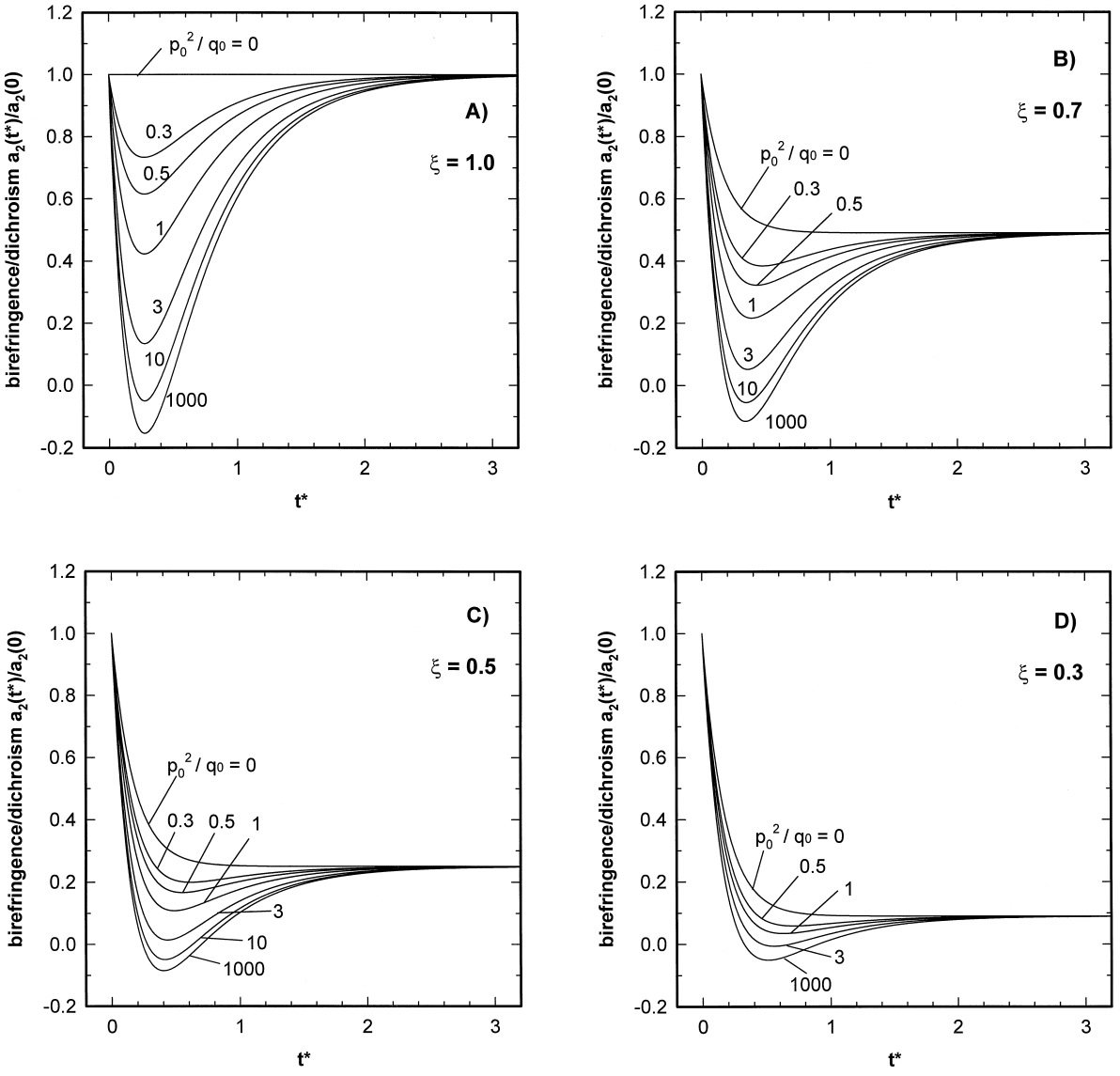

Fig. 3. Predicted birefringence/dichroism of rigid ellipsoidal macromolecules with different electrooptic properties (different p_0^2/q_0) in solution and subjected to an asymmetric reversing electric field. The birefringence/dichroism during the reversed is shown for a symmetry parameter ξ equal to (A) 1.0, (B) 0.7, (C) 0.5 and (D) 0.3. The birefringence/dichroism is shown as a function of the dimensionless variable $t^* = D_R t$ and is normalised to one at the time of field reversal.

Fig. 4 shows plots of the minimum value of $a_2(t^*)/a_2(0)$ as a function of p_0^2/q_0 for $\xi = 1.0$, 0.7, 0.5 and 0.3. This graph shows that the reversing pulse method is most accurate for $\xi = 1.0$, i.e., for symmetric a reversing pulse, and for values of p_0^2/q_0 in the range 0.2–10. For smaller values of ξ, the accuracy decreases significantly, and for $\xi = 0.3$ the obtainable estimates of p_0^2/q_0 are quite uncertain unless the signal-to-noise ratio of the electrooptic data is very high.

It is also possible to obtain estimates of p_0^2/q_0 using non-linear regression where p_0^2/q_0 and the rotational diffusion coefficient D_R are selected as the parameters to be adjusted to give best fit between the experimental

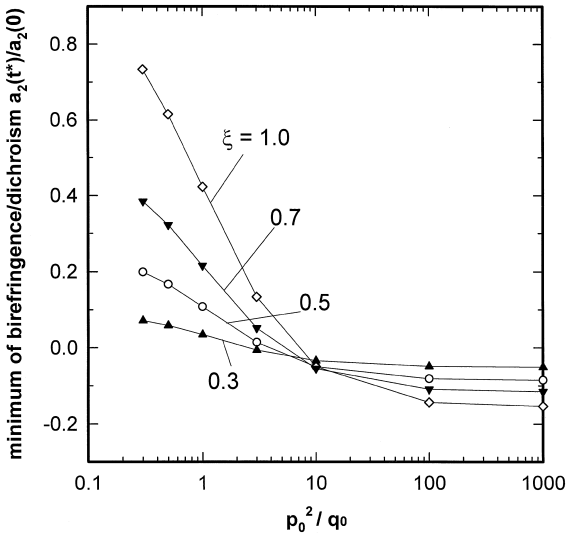

Fig. 4. Predicted relationship between the birefringence/dichroism minimum value of rigid ellipsoidal macromolecules in solution and their electrooptic properties described by p_0^2/q_0. The solution is subjected to an asymmetric reversing electric field. The birefringence/dichroism minimum after field reversal is calculated for a symmetry parameter ξ equal to 1.0 (◇), 0.7 (▽), 0.5 (○) and 0.3 (△). The birefringence/dichroism at field reversal is normalised to one.

data and the theoretical predictions of the birefringence/dichroism according to Eq. (17). In some cases this may give more accurate estimates than the simple approach outlined above, but also when non-linear regression is used there is a general trend towards less accurate estimates of p_0^2/q_0 as ξ becomes smaller and/or as the electrooptic signal-to-noise ratio decreases. An advantage of fitting Eq. (17) to the experimental data is that non-ideal electric field pulse (Eqs. (42)–(44)) may easily be accounted for.

To demonstrate the possibility of including non-zero reversal times of the electric field pulse, a numerical solution of Eq. (17) using the expressions in Eqs. (42)–(44) for $E(t)$, $p(t)$ and $q(t)$, was carried out using the fourth-order Runge–Kutta algorithm. The results are shown in Fig. 5 for two values of the symmetry factor ξ and values of p_0^2/q_0 ranging from 0 to 10. The decay parameters of $E(t)$ used in the analysis was determined from a least squares fit by two exponentials ($N = 2$ in Eq. (42)) to experimental curves with different symmetry factors ξ (see e.g., Figs. 6 and 7). When the electric field amplitude at field reversal was normalised to one, the best fits were found to be $\tau_1 = 18$ ns, $\tau_2 = 200$ ns, $c_1 = 1.1$ and $c_2 = 0.26$ when ξ was 0.36 and $\tau_1 = 13$ ns, $\tau_2 = 190$ ns, $c_1 = 1.2$ and $c_2 = 0.26$ when ξ was 0.46. There is no qualitative difference between these curves compared to the ones obtained with ideal electric field pulse reversal (Fig. 3); molecules with a large permanent dipole moment compared to the induced dipole moment show the deepest birefringence minimum.

4.2. Characteristics of the asymmetric reversing electric pulses across the Kerr cell

Asymmetric reversing electric pulses are generated when the resistive load impedance R is smaller than the characteristic resistive impedance Z of the coaxial cable. The symmetry parameter of the reversing electric pulse, ξ, defined by Eq. (35) equals [7,8]

$$\xi = \frac{Z - R}{Z + R} \tag{45}$$

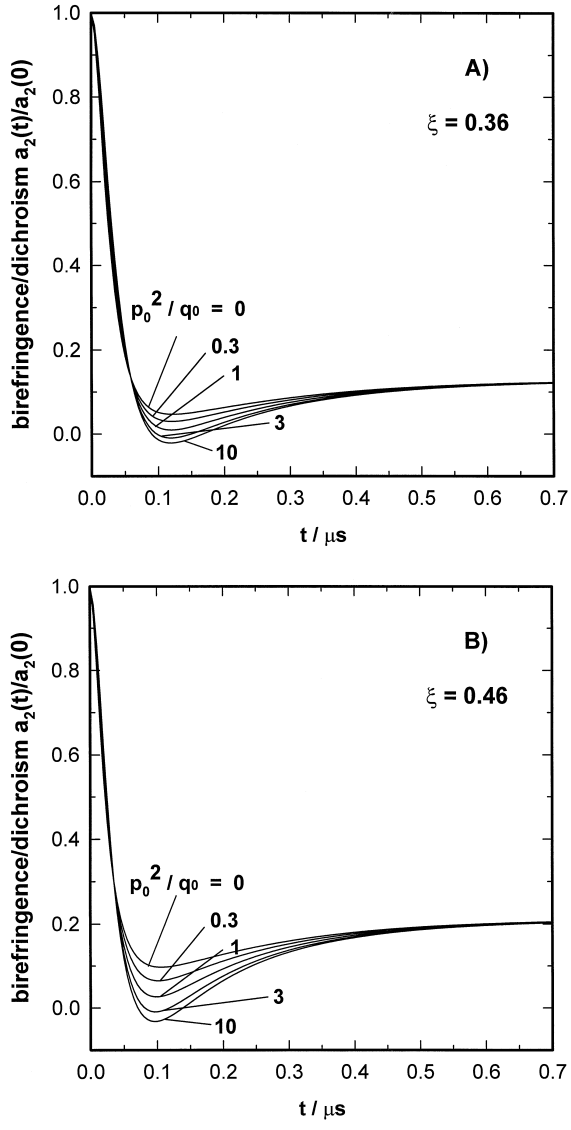

Fig. 5. Birefringence/dichroism predicted by numerical integration of Eq. (17) for solutions containing rigid ellipsoidal macromolecules with different electrooptic properties (different p_0^2/q_0) and subjected to an asymmetric reversing electric field with non-zero reversal time (decay characteristics of the electric field described in text). The birefringence/dichroism during the reversed pulse is shown for a symmetry parameter of (A) $\xi = 0.36$ and (B) $\xi = 0.46$. To facilitate comparison to experimental results (see Fig. 8), the curves are presented on real time scale,263 $t = t^*/D_R$, using a value of $D_R = 6.7\times10^7\ s^{-1}$.

When $\xi = 1$, the pulse in the cable is totally reflected and the reversing pulse across the Kerr cell is symmetric. When $\xi = 0$, the pulse is totally absorbed and the electric pulse across the Kerr cell is a single, rectangular pulse. This is why parameter ξ is also called the reflection parameter [7,8].

The expression for the load impedance R equals

$$\frac{1}{R} = \frac{1}{R_K} + \frac{1}{R_C} + \frac{1}{R_D} \tag{46}$$

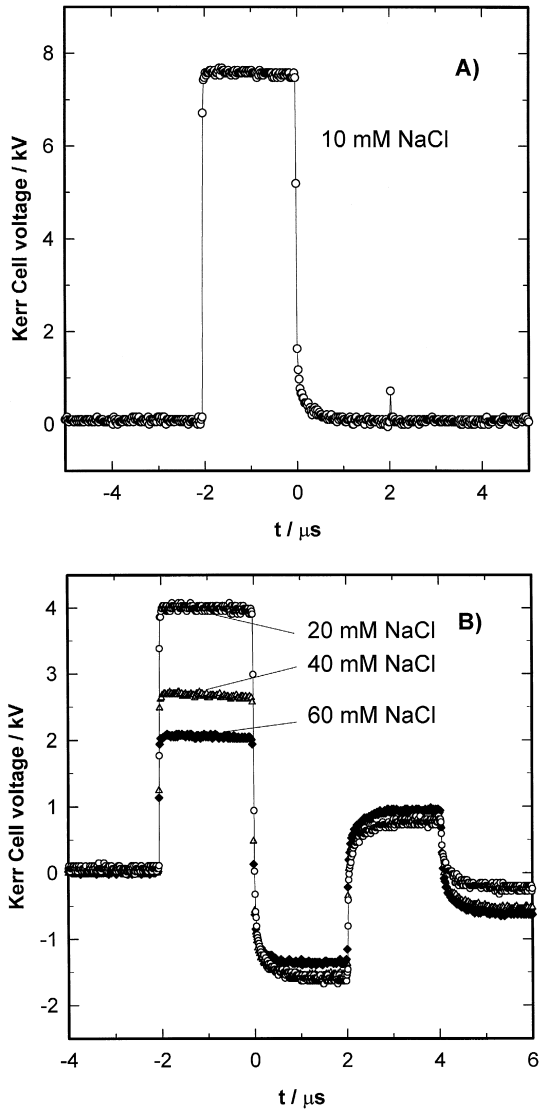

Fig. 6. Kerr cell voltage–time profiles during coaxial cable discharge when the Kerr cell is filled with water. When (A) a 10 mM NaCl solution circulates through the compensation cell, a single rectangular pulse is generated. When the NaCl concentration equals (B) 20 mM (○), 40 mM (△) or 60 mM (◇), asymmetric reversing electric pulses are generated. The signals were sampled every 20 ns and the coaxial cable was initially charged to 15 kV.

where R_K is the Kerr cell resistance, R_C the compensation cell resistance and R_D the voltage divider resistance network. The resistance R_D is large compared to R_K or R_C and is therefore neglected in our further calculations of R. A fraction equivalent to 5.5×10^{-4} of the voltage across the Kerr cell is monitored on the oscilloscope. The resistance R_K equals

$$R_K = \frac{1}{\sigma_K(T,c)} \frac{l}{A} \tag{47}$$

where $\sigma_K(T,c)$ is the sample conductivity and depends on the temperature T and the salt concentration c of the sample. The resistance of the cylindrical compensation cell equals

$$R_C = \frac{1}{\sigma_C(T,c)2\pi h}\ln\frac{b}{a} \tag{48}$$

where $\sigma_c(T,c)$ is the conductivity of the electrolyte in the compensation cell. In the set-up used in the work reported here the electrode separation l of the Kerr cell equals 4.0 mm and the sample cross-sectional area A equals 150 mm^2. The radius a of the inner cylinder equals 11 mm and the radius b of the outer one equals 16 mm. The length h of the cylinder equals 10 mm. For further technical details, see Bjørkøy [14].

When the Kerr cell is filled with water, i.e., when R_K is very large, a value $R_C \sim 50\ \Omega$ is required to obtain impedance matching. According to Eq. (48), this corresponds to a salt concentration of about 10 mM NaCl at 20°C. Increasing the salt concentration results in impedance mismatch and an asymmetric reversing pulse in agreement with the predictions of Eq. (45). The amplitude of the reversing pulse relative to the first pulse (ξ) may be increased by reducing the value of R (see Eq. (45)). The theoretical limit $\xi = 1$ can be obtained by choosing $R = 0$, but for this value the amplitude of the electric pulse vanishes. The amplitude of the first electric pulses equals $V = V_{HV}R/(R+Z)$, where V_{HV} equals the initial cable high voltage. Use of Eq. (45) further yields $V = V_{HV}(1-\xi)/2$. For given value of the initial coaxial cable voltage, the reversing pulse asymmetry is therefore obtained on the expense of the amplitude of the electric pulses. For some applications this may have important design implications.

Fig. 6 shows the experimental voltage–time profiles for different salt conditions. When the salt concentrations of the compensation chamber are 10, 20, 40 and 60 mM NaCl, respectively, the corresponding resistances given by Eqs. (46) and (48), equal 50, 26, 14 and 9 Ω. The symmetry parameters predicted from Eq. (45) equal 0, 0.32, 0.56 and 0.70, respectively. The symmetry parameters calculated from the voltage–time profiles in Fig. 6 equal 0, 0.43, 0.61 and 0.72, respectively, which shows adequate agreement between observed and calculated

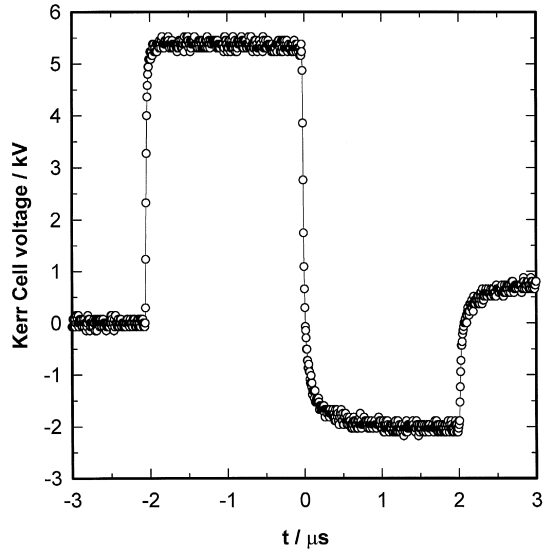

Fig. 7. Kerr cell voltage–time profile during coaxial cable discharge when the Kerr cell is filled with spectrin Dα14 (0.7 mg/ml) in a 5 mM HEPES, pH 7.35/1 mM NaCl solution at 4°C. The concentration of NaCl in the compensating electrolyte was 25 mM. The symmetry parameter ξ was measured and found to be 0.36. The signal was sampled every 5 ns and the coaxial cable was initially charged to 18 kV.

values. The observed reduction of the amplitude of the first electric pulse also are in good agreement with predicted values.

When the compensation cell is filled with water, i.e., when R_C is very large, R_K must be equal to 50 Ω in order to obtain impedance matching. If the sample temperature is 4°C, as is the case in our experiments, the sample salt concentration should be 80 mM NaCl, according to Eq. (47). Higher salt concentrations will result in reversing electric pulses across the Kerr cell when the coaxial cable is discharged. For higher temperatures the salt concentration must be lowered when a single rectangular pulse across the Kerr cell is required.

When a voltage U is maintained across the Kerr cell during the time Δt, the associated temperature elevation ΔT is given by

$$\left(U^2/R_K\right)\Delta t = mc_p\Delta T \tag{49}$$

where m is the sample mass and c_p is the heat capacity of the sample solution. Under the experimental conditions described here, the temperature elevation for single cable discharge is less than 0.05°C.

The NaCl concentration of the compensating electrolyte used in the experiments reported here is 25 ± 5 mM. This corresponds to $R_C = 25 \pm 5$ Ω according to Eq. (48). The sample buffer is 5 mM HEPES, pH 7.35/1.5 ± 0.5 mM NaCl, yielding $R_K \sim 2$ kΩ. According to Eq. (46), the load impedance $R = 25 \pm 5$ Ω and the symmetry parameter ξ predicted by Eq. (45) equals 0.33 ± 0.01.

Fig. 7 shows the reversing excitation pulse applied to the spectrin Dα14 sample. The electric field amplitude across the Kerr cell is 13.6 kV/cm for the first excitation pulse and −5.0 kV/cm for the reversed pulse, yielding an observed symmetry parameter $\xi = 0.37$ in agreement with the predicted value.

4.3. Birefringence of spectrin segment Dα14 in asymmetric reversing electric field

A small fraction of the spectrin segment Dα14 associate spontaneously into dimers during the preparation. This dimerization is reversible, but appears to be kinetically-trapped at low temperatures [19]. When the monomer-containing peak was reloaded on the gel filtration column after a storage of 24 or 48 h at 4°C, no dimer-containing peak was observed. Because all our birefringence measurements were carried out at the latter temperature, the presence of dimers during our measurements is expected to be negligible. After the thrombin cleavage step, the purity of the spectrin segment solution was checked using gel electrophoresis. The result shows a single band with a molecular weight of 12 kDa, in agreement with the published molecular weight of the protein sample.

Experimental electric birefringence data for Dα14 spectrin are shown in Fig. 8. The birefringence data were calculated employing the equations valid for analysis of data obtained in the linear detection mode [4].

Fig. 8B shows fitting of theoretical curves to the experimental birefringence data. The broken line in Fig. 8B represents the best fit of Eq. (39), that is, assuming zero reversal time of the external electric field pulse, and this fit was obtained using $p_0^2/q_0 = 3.5$ and $D_R = 4.2 \times 10^6$ s^{-1} ($\tau = 1/6\ D_R = 40$ ns). The value of 0.36 of the symmetry parameter ξ was used, as measured from the electric field pulse profile in Fig. 7. The solid line represents the best fit of Eq. (17), which takes into account non-ideality of the electric field pulse. The decay characteristics (Eq. (42)) of the electric field reversal used in the analysis was as described earlier for $\xi = 0.36$: $\tau_1 = 18$ ns, $\tau_2 = 200$ ns, $c_1 = 1.1$ and $c_2 = 0.26$. Using the fourth order Runge–Kutta numerical integration algorithm to solve Eq. (17) numerically, the best fit was obtained with $p_0^2/q_0 = 3.0$ and $D_R = 6.7 \times 10^6$ s^{-1} ($\tau = 1/6\ D_R = 25$ ns). For one single spectrin segment, the decay constant is expected to be ≤ 25 ns at 4°C [21]. Hence, a fit of Eq. (39) to the electrooptic signal yields over-estimated values of τ when the electric pulse actually is non-ideal.

The maximum DC voltage at which the coaxial cable pulse generator (Fig. 2) can operate equals 18–20 kV. Because the pulse height across the Kerr cell is only a fraction of this maximum when asymmetric electric

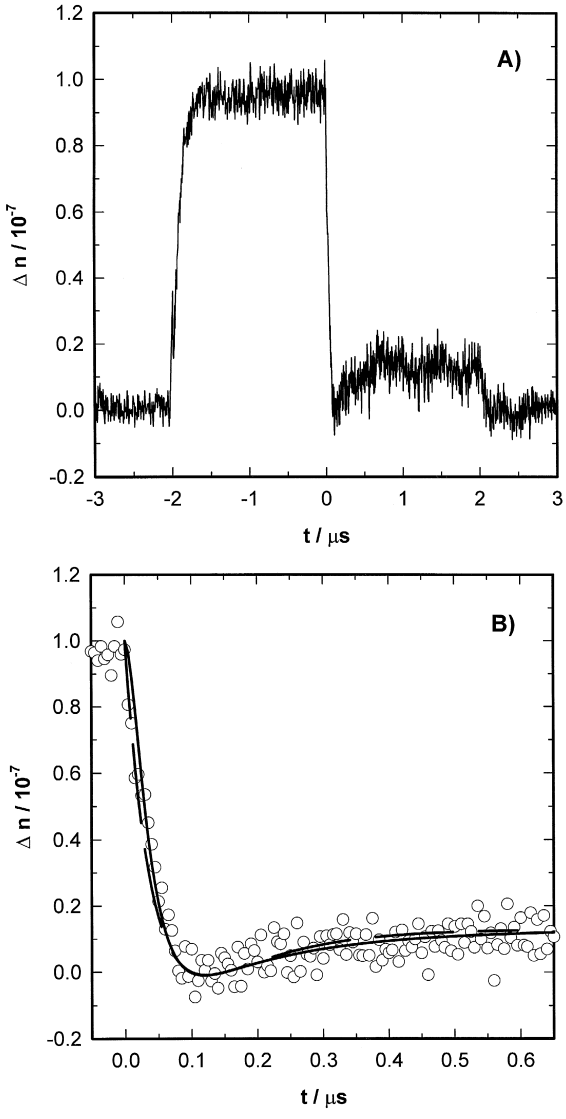

Fig. 8. Electric birefringence signal of spectrin Dα14 subjected to the non-ideal asymmetric reversing electric field pulse depicted in Fig. 7 and included to demonstrate the experimental feasibility of this new approach. The segment concentration is 0.7 mg/ml in 5 mM HEPES, pH 7.35/1 mM NaCl. The linear detection mode was used. The contribution of the solvent was subtracted from the total electrooptic signal. The data were obtained by averaging the electrooptic signals associated with 11 asymmetric pulses and by sampling every 5 ns. (A) Plot of the complete electrooptic signal using the same time scale as in Fig. 7. (B) Signal (○) after pulse reversal shown with larger time resolution. The theoretical predictions of the birefringence according to Eq. (39) (broken line) and Eq. (17) (solid line) are shown, assuming ideal and non-ideal electric field pulses, respectively.

pulses are generated, our current set-up—when used in asymmetric reversing electric pulse mode—is not capable of generating adequate signal-to-noise ratio birefringence data of spectrin Dα14. The experimental electrooptic data for spectrin segments are therefore included here only to demonstrate the feasibility of using asymmetric reversing electric pulses for studying the characteristics of small macromolecules and not to present quantitative results.

5. Conclusion

We have succeeded in deriving the analytic expressions needed for quantitative determination of the ratio between the permanent and the induced electric dipole moments of rigid macromolecules when the electrooptic data have been obtained employing reversing electric pulses with given asymmetry. Our analysis is valid only in the thermal domain. An alternative method—which can also be applied to strong electric field pulses—consists of employing Brownian dynamics simulations as described by Carrasco Gómez et al. [22]. However, this approach in general requires significantly more computer time and does therefore presently represent a less attractive alternative.

The described experimental technique for obtaining asymmetric reversing electric field pulses together with the presented theoretical analysis provide an independent alternative approach to obtain estimates of the electric dipole moments of small proteins and other small macromolecules with rotational relaxation times down to 10–20 ns and in the presence of as much as 0.1 M NaCl. The only significant drawback of the new approach appears to be the need for an initial voltage across the coaxial cable that may be more than twice the amplitude of the strongest component of the generated asymmetric reversing electric pulse.

Acknowledgements

We gratefully acknowledge receiving from Dr. Daniel Branton *Escherichia coli* strain 71-18 expressing segment 14 of *Drosophila* α-spectrin. His generous hospitality in allowing one of us (A.B.) to stay in his laboratory to learn the techniques necessary to take full advantage of this strain, is most appreciated. This work was supported by grant nos. 100570/410 and 425.91/003 from the Research Council of Norway and grant HL 17411 from NIH.

References

[1] J.G. Kirkwood, J.B. Shumaker, Proc. Natl. Acad. Sci. U.S.A. 38 (1952) 855–862.
[2] J. Antosiewicz, Biophys. J. 69 (1995) 1344–1354.
[3] I. Tinoco, K. Yamaoka, J. Am. Chem. Soc. 63 (1959) 423–427.
[4] E. Fredericq, C. Houssier, Electric Dichroism and Electric Birefringence, Clarendon Press, Oxford (1973) pp. 1–219.
[5] K. Ueda, M. Nomura, K. Yamaoka, Biopolymers 22 (1983) 2077–2090.
[6] T. Schönknecht, D. Porschke, Biophys. Chem. 58 (1996) 21–28.
[7] G.W. Hoffman, Rev. Sci. Instrum. 42 (1971) 1643–1647.
[8] H.H. Grünhagen, Entwiklung einer e-feldsprung-apparatur mit optischer detektion und ihre anwendung auf die assoziation ampliphiler elektrolyte (Ph.D thesis), Technische Universität Carlo-Wilhelmina, Braunschweig, 1974.
[9] A. Szabo, M. Haleem, D. Eden, J. Chem. Phys. 85 (1986) 7472–7479.
[10] K. Yamaoka, M. Tanigawa, R. Sasai, J. Chem. Phys. 101 (1994) 1625–1631.
[11] P.H. Benoit, Ann. Phys. 6 (1951) 561–609.
[12] I. Tinoco, J. Am. Chem. Soc. 77 (1955) 4486–4489.
[13] A. Bjørkøy, A. Elgsaeter, A. Mikkelsen, Biophys. Chem. (1998) submitted.
[14] A. Bjørkøy, An electrooptic study of cloned spectrin segments and native Spectrin (Dr. Ing. thesis), Norwegian University of Science and Technology, NTNU, Trondheim, 1997.
[15] D. Porschke, A. Obst, Rev. Sci. Instrum. 62 (1991) 818–820.
[16] C.T. O'Konski, Molecular Electro-Optics, Part I: Theory and Methods, Marcel Dekker, New York, 1976.
[17] W. Oppermann, Untersuchungen zur molekulare gestalt gelöste polyelektrolyte mit der methode der elektrischen doppelbrechnung (PhD. thesis), Matematisch-Naturwissenshaftlichen Fakultät der Technischen Universität Clausthal, Clausthal, 1986.
[18] E. Winograd, D. Hume, D. Branton, Proc. Natl. Acad. Sci. U.S.A. 88 (1991) 10788–10791.
[19] G.B. Ralston, T.J. Cronin, D. Branton, Biochemistry 35 (1996) 5257–5263.
[20] A. Elgsaeter, Biochim. Biophys. Acta 536 (1978) 235–244.
[21] P. Skjetne, K.D. Knudsen, J. Garcia de la Torre, A. Elgsaeter, Macromol. Theory Simul. 4 (1995) 253–275.
[22] B. Carrasco Gómez, A. Pérez Belmonte, M.C. López Martìnez, J. Garcìa de la Torre, J. Phys. Chem. 100 (1996) 9900–9905.